

# Robust Obstacle Segmentation based on Topological Persistence in Outdoor Traffic Scenes

Chunpeng Wei\*, Qian Ge\*, Somrita Chattopadhyay\*, and Edgar Lobaton\*

\*Department of Electrical and Computer Engineering

North Carolina State University, Raleigh, North Carolina 27695–7911

Email: cwei2@ncsu.edu, qge2@ncsu.edu

schatto2@ncsu.edu, edgar.lobaton@ncsu.edu

**Abstract**—In this paper, a new methodology for robust segmentation of obstacles from stereo disparity maps in an on-road environment is presented. We first construct a probability of the occupancy map using the UV-disparity methodology. Traditionally, a simple threshold has been applied to segment obstacles from the occupancy map based on the connectivity of the resulting regions; however, this outcome is sensitive to the choice of parameter value. In our proposed method, instead of simple thresholding, we perform a topological persistence analysis on the constructed occupancy map. The topological framework hierarchically encodes all possible segmentation results as a function of the threshold, thus we can identify the regions that are most persistent. This leads to a more robust segmentation. The approach is analyzed using real stereo image pairs from standard datasets.

## I. INTRODUCTION

In recent years, there has been significant development in the sector of intelligent driver assistance systems and autonomous vehicles in order to enhance safety by monitoring the on-road environment. One of the foremost issues that needs to be addressed for these Advance Driver Assistance Systems (ADAS) is the interpretation of surroundings of the ego vehicle, i.e. dynamic scene analysis and on-road obstacle detection. Recently, vision-based approaches for traffic-scene analysis have become an increasingly popular research area. In this paper, we focus on the problem of segmentation of obstacles in a disparity map obtained from a stereo-vision system. Real-time computation of dense disparity maps [1] has made stereo-vision an alternative to higher cost LIDAR systems. A driving scene analysis system typically extracts the road surface, segments the obstacles from the road, and computes the position of the obstacles relative to the ego vehicle.

The current state-of-the-art for solving this problem relies on parameter values that are carefully selected in order to provide good performance. Often these parameters rely on threshold values for segmentation of images. However, sensitivity of the detection results to these parameters can be a big concern. Small changes in threshold values can lead to large variations in the segmentation of the images. In this paper, we introduce a novel methodology for characterizing the sensitivity of a segmentation result based on persistent topology, and introduce an approach for robust obstacle detection.

Fig. 1 provides an overview of our methodology. This work builds on recent advances in ground segmentation and obstacle detection for safe autonomous driving. In particular, we employ an efficient UV-disparity approach to classify a 3D traffic scene into a ground plane and obstacles. Then, an occupancy grid is constructed to enable segmentation of the obstacles. Finally, we apply a topological persistence technique on the occupancy map to perform robust obstacle detection. The analysis of this method shows how this approach improves robustness of the detection results.

A fundamental difference between our approach and other existing approaches is its hierarchical nature. Topological persistence based segmentation does not rely on a single threshold value; instead, it keeps track of all the clustering

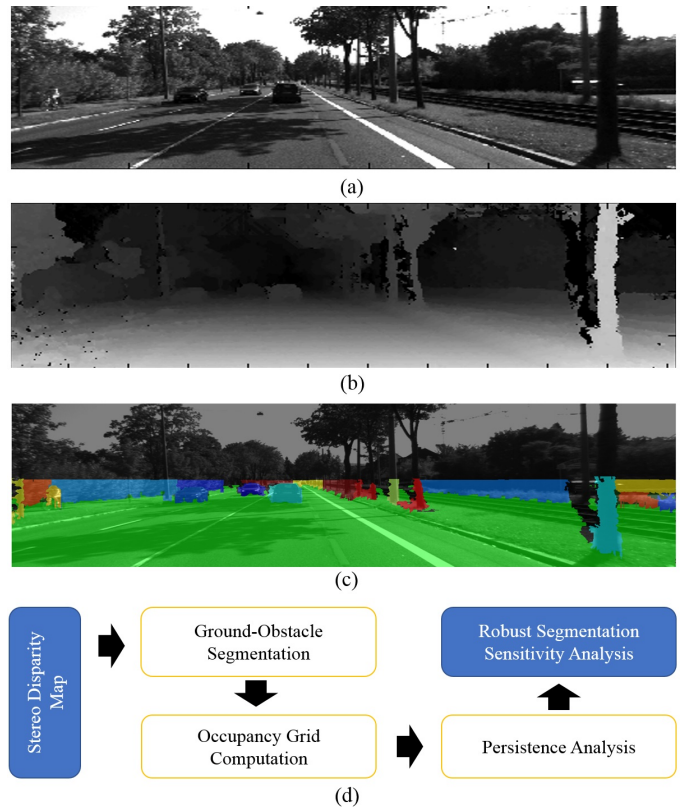


Fig. 1. Our Methodology. (a) Grayscale image, (b) Disparity depth map, (c) Robust segmentation results, and (d) Flowchart of the proposed methodology.

\*This work was supported by the National Science Foundation under award CNS-1239323.

results, corresponding to different thresholds. This is essentially providing a hierarchical clustering. A key advantage of our approach over traditional techniques is that the algorithm can be tuned for better performance through a few intuitive parameters leading to results that are less sensitive than simple thresholding. The proposed method also provides us with a persistence diagram that gives a compact visual representation of segmentation result corresponding to different threshold values. By analyzing this diagram, we can choose meaningful merging parameters for our segments and can also get a sense of the stability of the number of clusters under different choices of persistence parameters.

The remainder of this paper is organized as follows. Section II gives an overview of the current state-of-the-art. A brief background on topological persistence is presented in section III. Section IV presents our obstacle segmentation approach based on UV-disparity computations. A detailed description of our methodology using persistence for obstacle segmentation is introduced in section V. Results and robustness analysis of our proposed method are discussed in section VI. Finally, section VII summarizes the paper and discusses future work.

## II. RELATED WORK

This section provides a brief overview of the state-of-the-art of different segmentation methods, specifically in the field of ADAS. We focus on the current state-of-the-art of stereo vision based approaches, which make use of disparity depth maps for scene understanding.

In [2], Chen et al. segment the stereo disparity map by employing a depth slicing technique and then, accurately mark the object boundaries using a region growing method to improve on-road obstacle segmentation. Another region growing technique for vehicle detection is suggested by Kormann et al. [3]. In the first step, vehicles, modeled as cuboids, are detected using mean shift clustering of planar segments. Then, a UV-disparity map is computed to generate hypotheses for vehicle appearance and disappearance.

Recently, Wang et al. have presented a method for robust obstacle detection and free space calculation based on efficient disparity map computation and G-disparity [4]. The obstacles are detected using UV-disparity maps and splines are used for the road model. In [5], Lefebvre et al. perform vehicle detection by applying mean shift segmentation directly on the 3D point cloud estimated from the dense disparity maps computed from a stereo pair.

Erbs et al., in [6], compute dynamic stixels from stereo disparity map and use the Dynamic Stixel World representation for efficient and compact one-dimensional modeling of real world 3D road scenes. Optimal segmentation is performed by means of dynamic programming. In [7], this group presents another method for traffic scene understanding and driver assistance system by incorporating a Bayesian segmentation approach. Stixel representation of images adds robustness to their algorithms and thus, their method works pretty well even in adverse weather conditions.

Dense disparity map based on-road obstacle detection is presented as a constrained optimization problem in [8]. The depth image, here, is segmented based on surface orientation

criterion. In [9], two new obstacle detection algorithms based on disparity map segmentation for applications in intelligent vehicle systems are presented. The first algorithm assumes that the obstacles are located almost parallel to the image plane and directly segments them using a robust model fitting method applied to the quantised disparity space. The second method employs some morphological operations, followed by a robust model fitting technique to separate the ground regions.

Lee et al., in [10], perform vehicle detection using a road feature and disparity histogram. Road features are extracted from v-disparity maps and localized obstacles are divided into multiple obstacles using a disparity histogram and remerged using four criteria parameters - the obstacle size, distance, angle between the divided obstacles, and the difference of disparity values. In [11], they present another stereo-vision based obstacle detection approach using UV-disparity map and bird's-eye view mapping.

Recently, map-based segmentation and navigation techniques for autonomous vehicles are also gaining popularity. In [12], Martinez et al. propose a mapping algorithm based on probabilistic and heuristic methods to classify and predict the areas around an autonomous robot. Another path planning method for mobile robots is presented in [13]. This paper employs an enhanced dynamic Delaunay Triangulation approach and a GPS tail technique for robot navigation. In [14], Posada et al. present a robust method of floor-obstacle segmentation for mobile robot navigation. The method relies on fusing opinions of multiple heterogeneous classifiers generated from different segmentation schemes like graph cut and region growing to improve the overall classification rate.

Some other papers on traffic scene analysis and obstacle detection have incorporated techniques like watershed segmentation [15], connected component analysis [16], plane-fitting and edge based segmentations [17]. Literature has also addressed several surveys on intelligent transportation systems [18], [19].

In this paper, we have aimed for robust road and obstacle segmentation problem using a persistence based analysis. The next section gives a detailed description of topological persistence.

## III. BACKGROUND

Topological Data Analysis [20] is a new field of study which employs tools from persistent homology theory [21].

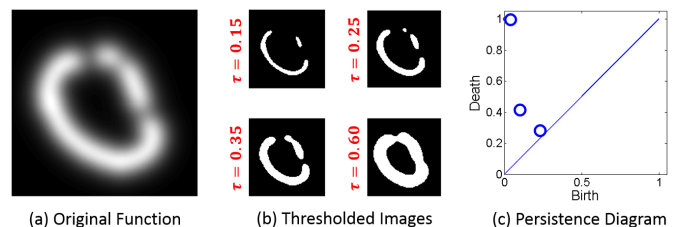


Fig. 2. Persistence Analysis. (a) Original grayscale image, (b) images after thresholding, and (c) persistence diagram. Each point in the diagram corresponds to clusters that are born and die at specific threshold values. Points near the diagonal are sensitive to small variations of the original image.

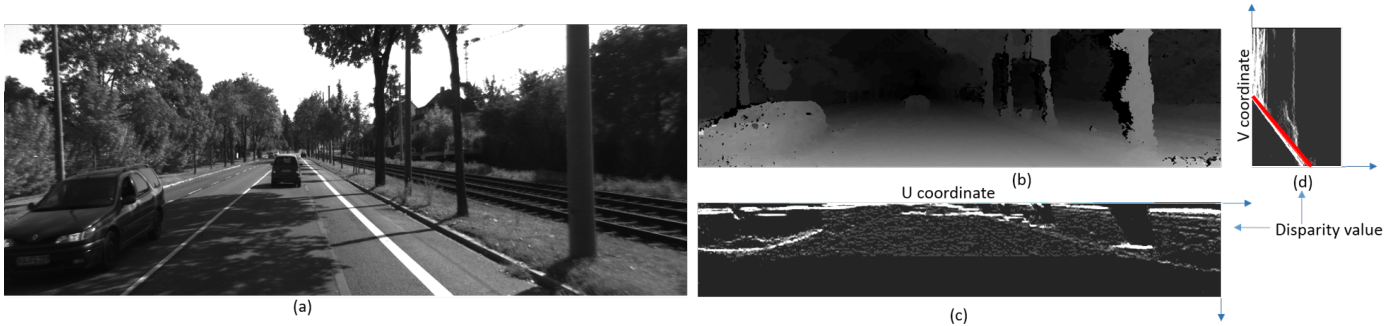


Fig. 3. Disparity Maps. (a) Grayscale image, (b) disparity map, (c) u-disparity and (d) v-disparity results. In the v-disparity map, the red line indicates the upper plane for road segmentation.

This analysis is commonly used for the extraction of topological attributes from functions or point cloud data. These features are captured in a compact visual representation called the *persistence diagram* [22]. Persistent homology has been used for segmentation [23] of natural images and clustering [24]. In this work, we make use of this framework to study the robustness of obstacle detection. This section provides a brief overview of some of the concepts of persistent homology in the context of image analysis. A comprehensive review of the topic can be found in [22].

Let us consider a function  $f : \mathbb{R}^2 \rightarrow [0, 1]$ . Given a threshold value  $\tau \in [0, 1]$ , we compute the upper level set  $S_\tau = f^{-1}[1 - \tau, 1]$ . As we will see later,  $f$  will represent the probability of obstacle occupancy at a location in front of the vehicle and  $S_\tau$  represents the set of detections if we choose a threshold value of  $\tau$ . Our goal is to analyze these detections and characterize their sensitivity to  $\tau$ .

The topological structures of the set  $S_\tau \subset \mathbb{R}^2$  can be summarized using the *Betti numbers*, which are the ranks of topological invariants called *homology groups*. The  $n$ -th Betti number,  $\beta_n$ , measures the number of  $n$ -dimensional cycles in the space (e.g., for a 2D space,  $\beta_0$  is equal to the number of *connected components* and  $\beta_1$  is equal to the number of *holes* in the space). The set  $\{S_\tau\}_{\tau \in [0, 1]}$  is referred to as a *filtration* and satisfies the following property:

$$S_{\tau_1} \subseteq S_{\tau_2} \quad \text{whenever} \quad \tau_1 \leq \tau_2. \quad (1)$$

Persistent homology computes the values of  $\tau$  for which topological features appear ( $b_n^k$ ) and disappear ( $d_n^k$ ) during a filtration, referred to as the *birth* and *death* values of the  $k$ -th feature in dimension  $n$  (e.g., connected components if  $n = 0$  and holes in the space if  $n = 1$ ). We will focus on connected components in order to characterize obstacle detections in this scenario. This information is encoded into a multiset of points ( $b_n^k, d_n^k$ ), called a *persistence diagram*. Each point is referred to as a *persistence interval* with corresponding length equal to  $d_n^k - b_n^k$ . Algorithms for the efficient computation of persistent homology can be found in [20], [25].

An example of a function  $f$ , sample sets  $S_\tau$ , and persistence diagram (for  $n = 0$ ) is shown in Fig. 2. There is a single cluster in the diagram for which its death time is much greater than its birth time (i.e., the point is furthest away from the diagonal). There is also one cluster near the

diagonal which only exists for a short persistence interval. The thresholded images illustrate that the small cluster is formed around  $\tau = 0.25$  and merges with a larger cluster soon after.

#### IV. UV-DISPARIITY BASED OBSTACLE SEGMENTATION

This section presents a road and obstacle segmentation approach based on prior work in the literature [31], which makes use of the UV-disparity map methodology.

##### A. UV-Disparity Map

We assume that a disparity map has been computed from a stereo pair of images from the vehicle. In our experiments, we make use of the *Semi Global Block Matching (SGBM)* technique [27]. This map can also be represented as a 3D point cloud where each point has coordinates  $(u, v, d)$ , where  $(u, v)$  represent the x-y coordinates in the image domain and  $d$  represents the disparity value. By projecting all the points to the ud-plane and the vd-plane and accumulating the overlapping points, we generate two new 2D images, called the u-disparity and the v-disparity [28] maps, respectively. Fig. 3 illustrates these maps for a stereo pair from the KITTI dataset [29].

##### B. Road Segmentation

We make use of the v-disparity map to segment the road from the obstacles. Under the assumption that the road can be approximated by a nearly-horizontal plane, then every row of the disparity map, that intercepts the road, will have its minimal value at the associated road pixels. That is, the points in the v-disparity map will be lower bounded by the points associated with the road. This lower bound can be approximated by a line in the v-disparity map as shown in Fig. 3.

In order to obtain a robust estimate for the ground plane, a line is fitted to the v-disparity map using robust regression techniques [30]. This line is referred to as  $g_{ground}(d)$ . We then use an appropriate threshold (based on height) to segment the road and obstacle pixels in the original image domain. In particular, the point  $(u, v, d)$  is labeled as an obstacle point if  $v$  is greater than

$$g_{lower}(d) = g_{ground}(d) + \left( \frac{\alpha_u h_g}{\alpha_v b} \right) d, \quad (2)$$

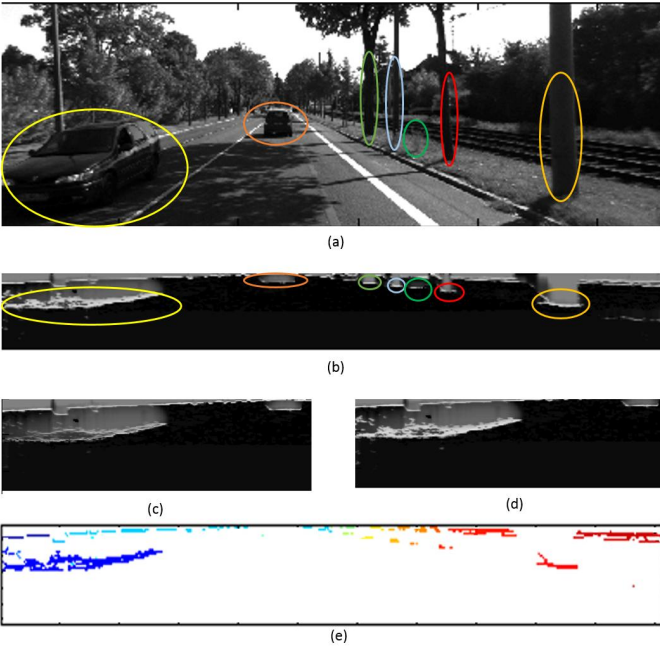


Fig. 4. Occupancy Results. (a) Grayscale image, (b) probability of occupancy map, (c) region of probability map for vehicle using original approach, (d) region of probability map for vehicle using modified approach, and (e) segmentation result using simple thresholding. Some corresponding regions are highlighted in (a) and (b). Plot (d) shows a better probability of detection using the modified approach.

where  $h_g$  is the height above the estimated ground plane used to identify road pixels,  $\alpha_u$  and  $\alpha_v$  represent the intrinsic focal length parameters of the camera in pixels, and  $b$  is the distance of the baseline for the stereo camera system. Fig. 3(d) shows  $g_{lower}$  as a red line in the  $v$ -disparity space.

### C. Occupancy Grid Computation

A probabilistic occupancy map in the  $u$ -disparity domain [31] is computed in order to enable the segmentation of objects. This map is obtained by using only those points in the disparity map that are above the ground plane and below a plane of height  $h_{max}$ , which specifies a maximum detection height for our approach.

Given a site  $s$  with coordinates  $(s_u, s_d)$  in the  $u$ -disparity domain, we define two binary random variables  $V_s$  and  $C_s$  which represent the visibility of this site ( $V_s = 1$  means that the site is visible) and the obstacle confidence ( $C_s = 1$  means that an obstacle is seen at  $s$ ). We can express the probability of occupancy,  $O_s$ , at site  $s$ , as

$$P(O_s) = \sum_{v,c} P(V_s = v, C_s = c) \cdot P(O_s | V_s = v, C_s = c), \quad (3)$$

where we define

$$\begin{aligned} P(O_s | V_s = 0, C_s = c) &= 0.5 \quad \forall c \in \{0, 1\} \\ P(O_s | V_s = 1, C_s = 1) &= 1 - P_{FP} \\ P(O_s | V_s = 1, C_s = 0) &= P_{FN} \end{aligned} \quad (4)$$

with  $P_{FP}$  and  $P_{FN}$  representing the false positive and false negative probabilities of occupancy detection respectively. We

assume independence between  $V_s$  and  $C_s$ , which leads to the need for expressions for  $P(V_s = v)$  and  $P(C_s = c)$ .

In order to compute these probabilities, we let  $N_P(s)$  be the total number of measured points in image domain at site  $s$ ,  $N_O(s)$  is the total number of obstacle points, and  $N_V(s)$  is the total number of visible points. These three quantities can be obtained from

$$\begin{aligned} A_P(s) &= \{(u, v) | u = s_u, v \in [g_{lower}(s_d), g_{upper}(s_d)]\} \\ A_O(s) &= \{(u, v) | I_D(u, v) = s_d\} \cap A_P(s) \\ A_V(s) &= \{(u, v) | I_D(u, v) \leq s_d\} \cap A_P(s) \end{aligned} \quad (5)$$

which leads to  $N_a(s) = |A_a(s)|$ , where  $a \in \{P, O, V\}$ ,  $I_D$  is the disparity map,  $(u, v)$  is a coordinate in the disparity image domain,  $g_{lower}$  and  $g_{upper}$  represent the  $v$ -coordinates of the pixels on the ground and the maximum height plane, as functions of the disparity values (i.e., these are the equations defining the lower and upper planes for obstacle detections).

The probability of visibility for the site  $s$  in  $u$ -disparity space is then defined as

$$P(V_s = 1) = \frac{N_V(s)}{N_P(s)}, \quad (6)$$

and the probability of confidence of observation as

$$P(C_s = 1) = 1 - e^{-\lambda \frac{N_O(s)}{N_V(s)}}, \quad (7)$$

where  $\lambda$  is a constant parameter. Fig. 4 shows the probability of occupancy results and highlights some corresponding regions in between the grayscale image and the occupancy map.

A scenario in which this approach does not seem to work that well is when surfaces of the obstacles observed are not vertical (e.g., the windshield of a vehicle). In this case, points of the same object are dispersed over various sites on the  $u$ -disparity map, leading to low probability of occupancy over a region in this space.

To resolve this problem, all the invisible points in the disparity space below a point that has already been identified as an obstacle are considered as obstacles. In other words, given

$$A_{IO}(s) = \{(u, v) | I_D(u, v) > s_d, \exists v', (u, v') \in A_O(s)\} \quad (8)$$

we redefine

$$A_O^{new}(s) = A_O(s) \cup (A_{IO}(s) \cap A_P(s)) \quad (9)$$

and use this quantity to update the value of  $N_O(s)$ . Fig. 4 shows the improvement on the probability of occupancy over the original method.

### D. Obstacle Segmentation by Threshold Value

The traditional approach for obstacle segmentation in the  $u$ -disparity domain is to apply a constant threshold to the occupancy grid and form a new binary obstacle map. Connected components from this binary map are regarded as separate obstacles. Fig. 4 shows a sample segmentation result.

Each obstacle detected in the  $u$ -disparity domain needs to be mapped back to the original image plane for display. This is done by taking a site  $s$  in the  $u$ -disparity space and identifying all points in the image domain with  $u$ -coordinate  $s_u$  and disparity  $s_d$  with the object label assigned to  $s$ .

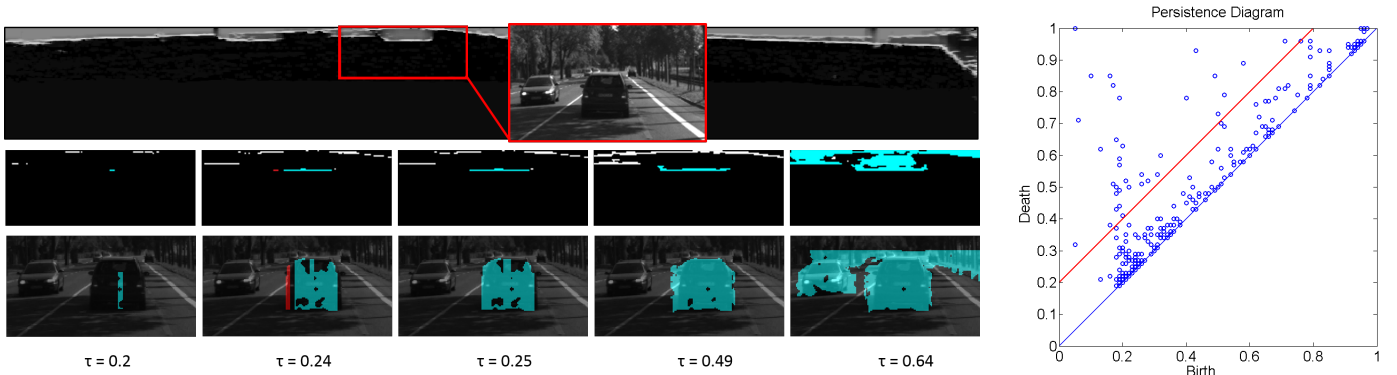


Fig. 5. Birth and death of connected components during filtration. First row on the left shows a part of the original image and the corresponding probability of occupancy map. Second row shows a connected component in cyan which corresponds to a car in the image space for five different values of  $\tau$ , and third row shows the corresponding regions in image space. On the right, the persistence diagram corresponding to the shown occupancy map. Each point indicates the lifespan of a connected component. The red line is the threshold line  $\gamma_{per} = 0.2$ . All the regions above this line have persistence interval greater than 0.2.

## V. EXTRACTING PERSISTENT REGIONS

Let us begin by defining

$$f(s) = P(O_s) \quad (10)$$

as the probability of occupancy function over the u-disparity space in order to draw a connection with the concepts introduced in Section III.

Segmentation of  $f$  via simple thresholding is fast and easy to implement. However, the proper threshold value may not be easily selected due to variations on the probability map attributed to the quality of the disparity map. The latter is affected by external and internal factors such as illumination and the texture of objects. Thus, the ideal threshold may change between images, even in the same video sequence. This simple type of segmentation is very sensitive to the choice of threshold value. As we will see in the experimental section, small variations in the threshold value can lead to a large number of regions introduced and removed. Furthermore, obstacles are associated with peaks in probability of the occupancy map  $f$ , for which there may not be a single threshold value that includes all these peaks without merging obstacle regions that are not supposed to be merged. In order to address all of these issues, we make use of topological persistence to generate a more robust segmentation.

Fig. 5 (left) illustrates the birth and death process of connected components during the filtration of upper level sets of  $f$ . At  $\tau = 0.2$ , the cyan region is born. Another region in red is also born at  $\tau = 0.24$  but dies at  $\tau = 0.25$ , because it merges with the cyan region which has an earlier birth time. The persistence interval of the red region is 0.01. At  $\tau = 0.49$ , the cyan region is still alive and its area increases. At  $\tau = 0.64$ , this region dies leading to a persistence interval of length 0.44. Note that by choosing regions with a persistence interval length greater than  $\gamma_{per} = 0.2$ , the cyan region would be selected, while the red region would be removed.

The birth and death of all regions obtained from  $f$  are captured in the persistence diagram, as displayed in Fig. 5 (right). Each point in the persistence diagram represents the lifespan of a region. Note that this diagram contains hierarchical information about the merging of these regions as a function of  $\tau$ . In order to obtain a robust segmentation of the

obstacles, we keep only those regions with persistence interval greater than  $\gamma_{per} = 0.2$ . This bound is illustrated by a red line in Fig. 5 (right). Finally, in order to obtain a labeling of the clusters in the u-disparity map, we need to determine the support of the selected persistent regions. However, since a region can exist over a range of values of  $\tau$ , its size can vary. In this case, we select the largest set of points for each region which is associated with the value of  $\tau$  before the region dies. The only problem with this assignment is that the support of the regions may be overlapping, in which case a point in the u-disparity space is assigned to the region with the lowest death time.

Fig. 6 illustrates the clustering result for  $\gamma_{per} = 0.2$ . We apply the same approach introduced in Sec. IV-D to illustrate the segmentation result in the image space.

## VI. RESULTS

The entire process is implemented in MATLAB on a 3.4 GHz computer with 16GB RAM. It takes approximately 9.5 seconds for a  $1242 \times 375$  image for  $\tau \in [0, 1]$ . We make use of stereo image pairs from the KITTI Vision Benchmark Suite [29], [32], [33] for analysis. For Occupancy grid computation,  $P_{FP} = 0.01$ ,  $P_{FN} = 0.05$ , and  $\lambda = 10$ . The persistence analysis is performed by varying  $\tau \in [0.1, 0.9]$  and letting  $\gamma_{per} = 0.2$  unless otherwise specified. For both the thresholding method and the proposed persistence analysis method, a simple morphological post-processing step is applied

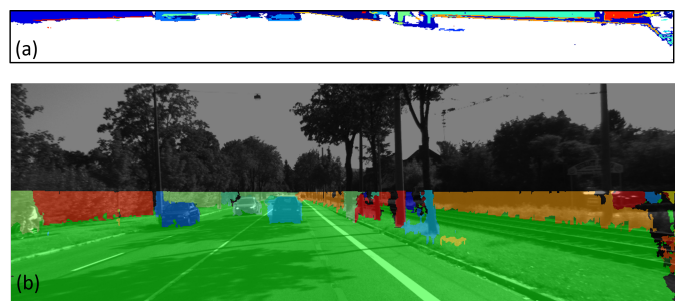


Fig. 6. Segmentation results. (a) Clusters in u-disparity space, and (b) their corresponding regions in image space.

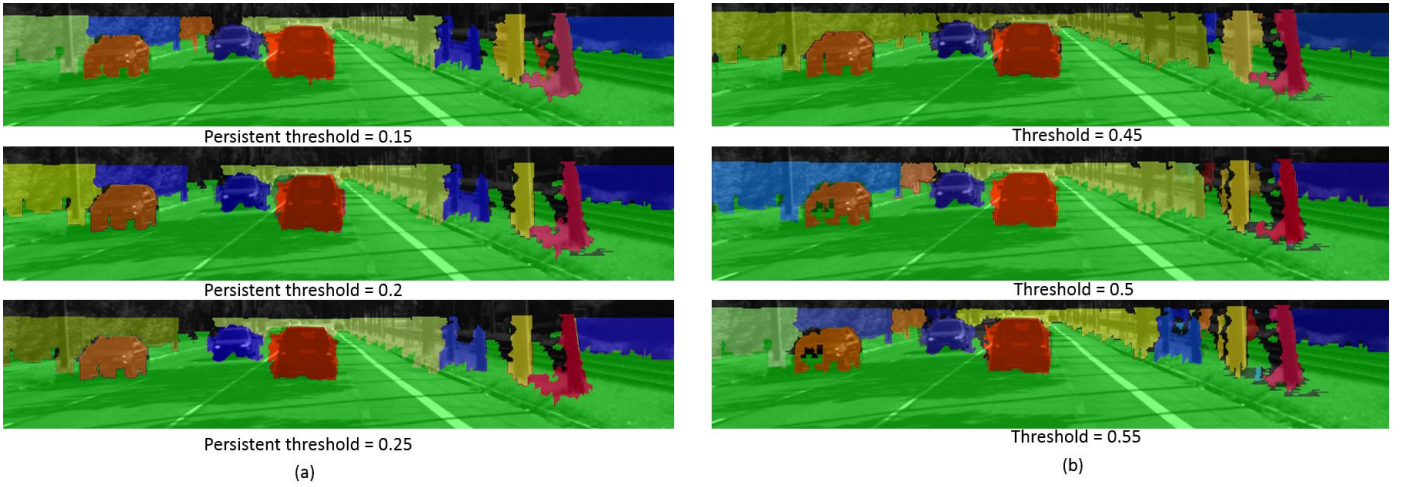


Fig. 7. Comparison between thresholding and persistence methods. (a) Results of persistence approach for  $\gamma_{per} = 0.15, 0.2$  and  $0.25$ . (b) Results of thresholding approach for  $\tau = 0.45, 0.5$  and  $0.55$ .

to the segmented images in order to remove the small detection regions as well the small gaps in the detection regions.

In this section, we compare the persistence method with the traditional thresholding method and analyze the effect of the persistence bound for our persistence method.

#### A. Comparing Thresholding and Persistence Method

Although thresholding is a simple solution for segmentation of the obstacles in the probability of occupancy map, it is highly sensitive to the choice of parameter value. On the other hand, the persistence based method performs an analysis for a range of threshold values and keeps track of all the resulting segmentations in a hierarchical fashion. We exploit this property to obtain a more robust outcome.

Fig. 7 provides sample results for both the thresholding and persistence methods. For thresholding,  $\tau$  is set to 0.45, 0.5 and 0.55. For persistence,  $\gamma_{per}$  is set to 0.15, 0.2 and 0.25. We picked these ranges in order to make the results for both methods comparable for the middle parameter value. It is

observed that even over this small range, thresholding causes significant variation in its output. In particular, there are several detection regions that appear and disappear on the right side of the image. On the contrary, the results for persistence are very consistent over a similar range of parameters.

We quantify the robustness of our method by analyzing how new regions are introduced and removed as parameters change for both methods. Fig. 8(a) and (b) illustrate how regions get added and removed by using the thresholding approach. These plots are histograms of the birth and death values of all the regions computed from the persistence analysis. Fig. 8(c) represents the total change on the number of regions as a function of threshold parameter  $\tau$ . When  $\tau$  changes from 0.45 to 0.5, around 30 regions are added or removed from the result, some of which are removed through post-processing. When it changes from 0.5 to 0.55, around 20 regions are added or removed. Fig. 8(d) shows the total number of regions as a function of  $\tau$ . We note that the sensitivity of the segmentation results cannot be observed from this plot, since regions are both added and removed making the net change on the number of regions small, but producing very different segmentation results.

Fig. 9 shows a similar analysis for persistence. In the case of persistence, increasing  $\gamma_{per}$  only gets rid of regions by merging them. The histogram of number of regions merged as a function of  $\gamma_{per}$  is shown in Fig. 9(a). In this case, changing  $\gamma_{per}$  from 0.15 to 0.2 or from 0.2 to 0.25 leads to less than

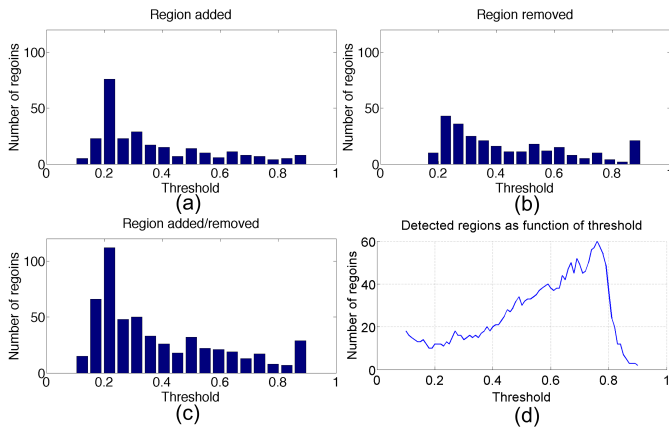


Fig. 8. Changes in detection regions for thresholding approach. (a) Number of regions added and (b) Number of regions removed as a function of  $\tau$ . (c) Total number of regions added or removed. (d) Total number of regions as a function of  $\tau$ . The bin size for (a)-(c) is 0.05.

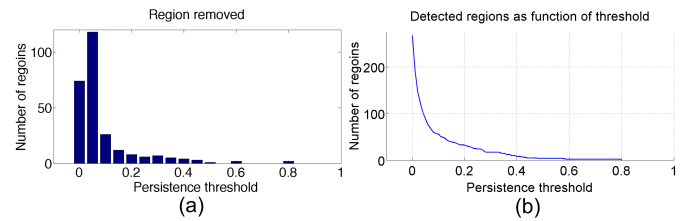


Fig. 9. Changes in detection regions for persistence approach. (a) Number of regions removed and (b) total number of regions as a function of  $\gamma_{per}$ . The bin size for (a) is 0.05.

10 regions removed or added. The total number of regions as a function of  $\gamma_{per}$  is shown in Fig. 9(b) which can be directly correlated with the histogram of regions removed. Both of these plots can be directly extracted from the persistence diagram.

### B. Effect of Persistence Bound

The persistence bound  $\gamma_{per}$  is used to select the most prominent regions in the hierarchical clustering of the data. This selection process can be visualized in the persistence diagram as selected features above a particular line (see Fig. 5

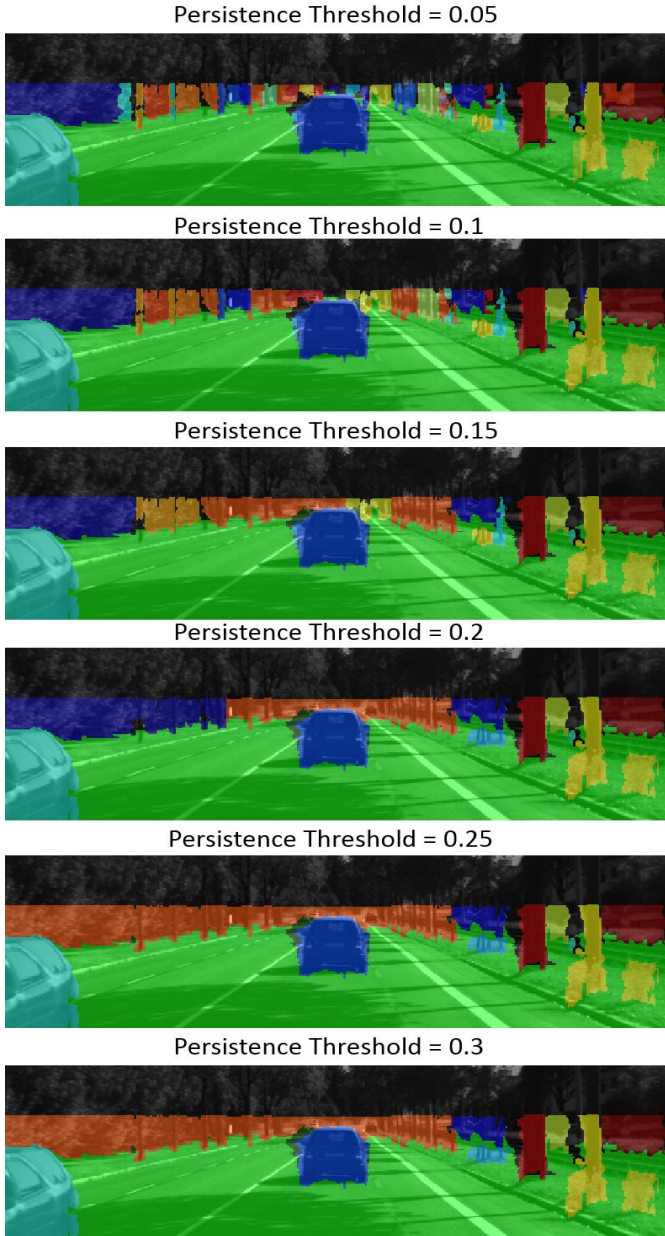


Fig. 10. Segmentation results for persistence bound  $\gamma_{per}$  ranging from 0.05 to 0.3. Bushes and trees are separated when  $\gamma_{per} = 0.05$  and 0.1. They are merged when  $\gamma_{per}$  increases from 0.1 to 0.2. When  $\gamma_{per} = 0.25$  and 0.3, the results are essentially unchanged. Note that two vehicles are always detected properly for all persistence thresholds.

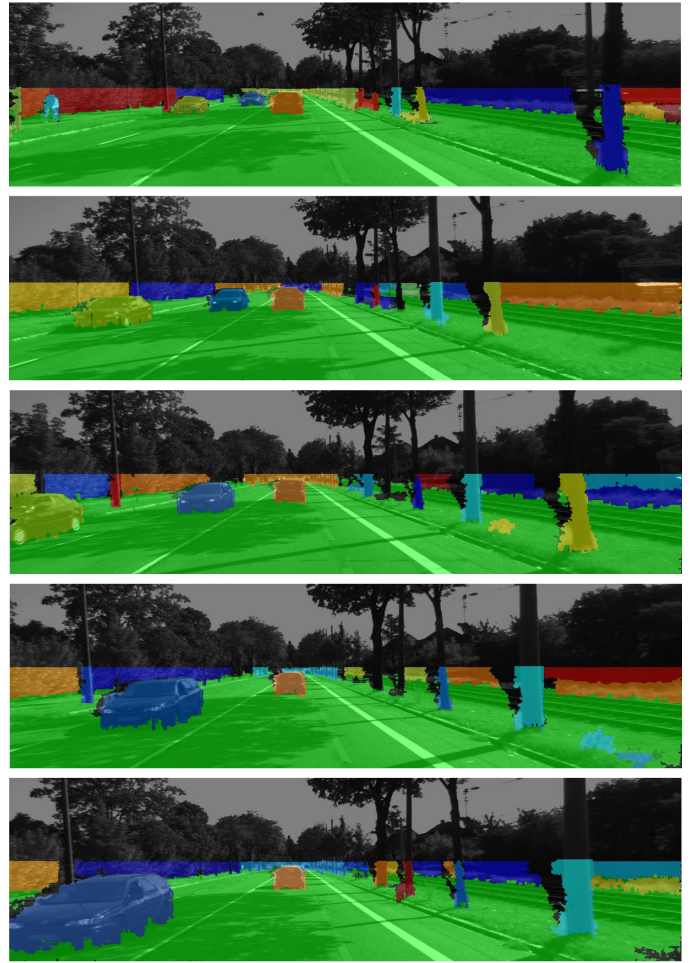


Fig. 11. Segmentation results. Results are performed by varying  $\tau \in [0.1, 0.9]$  and letting  $\gamma_{per} = 0.2$  in this case. Cars, trees and bushes can be detected and segmented on each frame, and in the first frame we also detected the person on the left side.

for an example). As the value of  $\gamma_{per}$  increases, the line moves up, allowing fewer but larger regions to be selected. This is due to the merging of some of these regions. During this process, obstacles which are close to each other in the image space will get merged first.

Fig. 10 illustrates the changes in the segmentation results as  $\gamma_{per}$  increases. When  $\gamma_{per} = 0.05$ , we can see that trees and bushes on both sides are divided into several small regions. When it increases to 0.25, trees on the left are merged into one region. The results are essentially unchanged between  $\gamma_{per} = 0.25$  and 0.3. The two vehicles are always detected and segmented properly between 0.05 and 0.3.

Fig. 11 shows several segmentation results using our methodology. It is observed that our approach is able to correctly segment ground from obstacles. Furthermore, obstacle detection and segmentation results are qualitatively good. Cars that are not too far from the ego vehicle are detected consistently as single regions. On the top image, the method is also able to detect an individual driving a bike. Also, most trees and bushes are detected and segmented properly on both sides of the road. While the bushes on the left side of the road are always detected, sometimes they will be split or merged

into a single region.

## VII. CONCLUSIONS AND FUTURE WORK

In this paper, we propose a robust road extraction and obstacle segmentation methodology from stereo disparity maps. We compute UV-disparity maps and an occupancy grid for easy obstacle segmentation and analyze the sensitivity of the segmentation results by using tools from persistent topology. This framework provides us with a persistence diagram that helps us explore all thresholding results in a hierarchical fashion and achieve a robust segmentation. The method has been tested on several stereo test images available from standard stereo databases and the results look promising.

In the future, we will continue our work to make the segmentation more robust and extend our approach to object recognition, classification and tracking. In particular, the entire persistent diagram can be used to track objects over time without throwing away potentially correct segmentation results and without relying on a single threshold value. Additionally, the choice of the persistence bound,  $\gamma_{per}$ , is also essential for compact visualization of the data.

## REFERENCES

- [1] W. Van Der Mark and D. M. Gavrila, "Real-time dense stereo for intelligent vehicles," *Intelligent Transportation Systems, IEEE Transactions on*, vol. 7, no. 1, pp. 38–50, 2006.
- [2] L.-C. Chen, X.-L. Nguyen, and C.-W. Liang, "Object segmentation method using depth slicing and region growing algorithms," in *International Conference on 3D Systems and Applications, Tokyo, Japan, 2010*, pp. 87–90.
- [3] B. Kormann, A. Neve, G. Klinker, W. Stechele *et al.*, "Stereo vision based vehicle detection," in *VISAPP (2)*, 2010, pp. 431–438.
- [4] Y. Wang, Y. Gao, A. Achim, and N. Dahnoun, "Robust obstacle detection based on a novel disparity calculation method and g-disparity," *Computer Vision and Image Understanding*, vol. 123, pp. 23–40, 2014.
- [5] S. Lefebvre and S. Ambellouis, "Vehicle detection and tracking using mean shift segmentation on semi-dense disparity maps," in *Intelligent Vehicles Symposium (IV), 2012 IEEE*. IEEE, 2012, pp. 855–860.
- [6] F. Erbs, A. Barth, and U. Franke, "Moving vehicle detection by optimal segmentation of the dynamic stixel world," in *Intelligent Vehicles Symposium (IV), 2011 IEEE*. IEEE, 2011, pp. 951–956.
- [7] F. Erbs, B. Schwarz, and U. Franke, "From stixels to objects: a conditional random field based approach," in *Intelligent Vehicles Symposium (IV), 2013 IEEE*. IEEE, 2013, pp. 586–591.
- [8] W. Miled, J. C. Pesquet, and M. Parent, "Robust obstacle detection based on dense disparity maps," in *Computer Aided Systems Theory—EUROCAST 2007*. Springer, 2007, pp. 1142–1150.
- [9] N. Gheissari and N. Barnes, "Road obstacle detection using robust model fitting," in *Field and Service Robotics*. Springer, 2006, pp. 43–54.
- [10] C.-H. Lee, Y.-C. Lim, S. Kwon, and J.-H. Lee, "Stereo vision-based vehicle detection using a road feature and disparity histogram," *Optical Engineering*, vol. 50, no. 2, pp. 027 004–027 004, 2011.
- [11] C.-H. Lee, Y.-C. Lim, S. Kwon, and J. Kim, "Stereo vision-based obstacle detection using dense disparity map," in *2011 International Conference on Graphic and Image Processing*. International Society for Optics and Photonics, 2011, pp. 82 853O–82 853O.
- [12] L. Martinez, M. Paulik, M. Krishnan, and E. Zeino, "Map-based lane identification and prediction for autonomous vehicles," in *Electro/Information Technology (EIT), 2014 IEEE International Conference on*. IEEE, 2014, pp. 448–453.
- [13] J. Chen, C. Luo, M. Krishnan, M. Paulik, and Y. Tang, "An enhanced dynamic delaunay triangulation-based path planning algorithm for autonomous mobile robot navigation," in *IS&T/SPIE Electronic Imaging*. International Society for Optics and Photonics, 2010, pp. 75 390P–75 390P.
- [14] L.-F. Posada, K. K. Narayanan, F. Hoffmann, and T. Bertram, "Ensemble of experts for robust floor-obstacle segmentation of omnidirectional images for mobile robot visual navigation," in *Robotics and Automation (ICRA), 2011 IEEE International Conference on*. IEEE, 2011, pp. 439–444.
- [15] T. Veit, "Connexity based fronto-parallel plane detection for stereovision obstacle segmentation," in *IEEE Int. Conf. on Robotics and Automation, Workshop on Safe Navigation in Open and Dynamic Environments: Applications to Autonomous Vehicles*, 2009.
- [16] Z. Khalid, E.-A. Mohamed, and M. Abdenbi, "Stereo vision-based road obstacles detection," in *Intelligent Systems: Theories and Applications (SITA), 2013 8th International Conference on*. IEEE, 2013, pp. 1–6.
- [17] X. Li, X. Yao, Y. L. Murphey, R. Karlsen, and G. Gerhart, "A real-time vehicle detection and tracking system in outdoor traffic scenes," in *Pattern Recognition, 2004. ICPR 2004. Proceedings of the 17th International Conference on*, vol. 2. IEEE, 2004, pp. 761–764.
- [18] S. Sivaraman and M. M. Trivedi, "Looking at vehicles on the road: A survey of vision-based vehicle detection, tracking, and behavior analysis," 2013.
- [19] R. A. Hadi, G. Sulong, and L. E. George, "Vehicle detection and tracking techniques: A concise review," *Signal*, 2014.
- [20] H. Edelsbrunner, D. Letscher, and A. Zomorodian, "Topological persistence and simplification," *Discrete and Computational Geometry*, vol. 28, no. 4, pp. 511–533, 2002. [Online]. Available: <http://dx.doi.org/10.1007/s00454-002-2885-2>
- [21] H. Edelsbrunner and J. Harer, "Persistent homology—a survey," *Contemporary mathematics*, vol. 453, pp. 257–282, 2008.
- [22] H. Edelsbrunner and J. Harer, *Computational Topology - an Introduction*. American Mathematical Society, 2010.
- [23] D. Letscher and J. Fritts, "Image Segmentation Using Topological Persistence," in *Computer Analysis of Images and Patterns*, ser. Lecture Notes in Computer Science. Springer Berlin Heidelberg, 2007, vol. 4673.
- [24] F. Chazal, L. J. Guibas, S. Y. Oudot, and P. Skraba, "Persistence-based clustering in riemannian manifolds," in *Proceedings of the Twenty-seventh Annual Symposium on Computational Geometry*, ser. SoCG '11. New York, NY, USA: ACM, 2011, pp. 97–106. [Online]. Available: <http://doi.acm.org/10.1145/1998196.1998212>
- [25] A. Zomorodian and G. Carlsson, "Computing persistent homology," in *Symp. on Computational geometry (SoCG)*. New York, New York, USA: ACM Press, 2004, pp. 249–274. [Online]. Available: <http://portal.acm.org/citation.cfm?doid=997817.997870>
- [26] M. Perrollaz, J.-D. Yoder, A. Spalanzani, and C. Laugier, "Using the disparity space to compute occupancy grids from stereo-vision," in *Intelligent Robots and Systems (IROS), 2010 IEEE/RSJ International Conference on*. IEEE, 2010, pp. 2721–2726.
- [27] H. Hirschmuller, "Stereo processing by semiglobal matching and mutual information," *Pattern Analysis and Machine Intelligence, IEEE Transactions on*, vol. 30, no. 2, pp. 328–341, 2008.
- [28] Z. Hu and K. Uchimura, "Uv-disparity: an efficient algorithm for stereovision based scene analysis," in *Intelligent Vehicles Symposium, 2005. Proceedings. IEEE*. IEEE, 2005, pp. 48–54.
- [29] A. Geiger, P. Lenz, C. Stiller, and R. Urtasun, "Vision meets robotics: The kitti dataset," *International Journal of Robotics Research (IJRR)*, 2013.
- [30] J. O. Street, R. J. Carroll, and D. Ruppert, "A note on computing robust regression estimates via iteratively reweighted least squares," *The American Statistician*, vol. 42, no. 2, pp. 152–154, 1988.
- [31] M. Perrollaz, J.-D. Yoder, A. Nègre, A. Spalanzani, and C. Laugier, "A visibility-based approach for occupancy grid computation in disparity space," *Intelligent Transportation Systems, IEEE Transactions on*, vol. 13, no. 3, pp. 1383–1393, 2012.
- [32] A. Geiger, P. Lenz, and R. Urtasun, "Are we ready for autonomous driving? the kitti vision benchmark suite," in *Conference on Computer Vision and Pattern Recognition (CVPR)*, 2012.
- [33] J. Fritsch, T. Kuehnl, and A. Geiger, "A new performance measure and evaluation benchmark for road detection algorithms," in *International Conference on Intelligent Transportation Systems (ITSC)*, 2013.